




# Advanced Turning Maneuver of a Many-Legged Robot Using Pitchfork Bifurcation

Shinya Aoi , *Member, IEEE*, Ryoe Tomatsu, Yuki Yabuuchi, Daiki Morozumi, Kota Okamoto, Soichiro Fujiki , *Member, IEEE*, Kei Senda , *Member, IEEE*, and Kazuo Tsuchiya

**Abstract**—Legged robots have excellent terrestrial mobility for traversing diverse environments and, thus, have the potential to be deployed in a wide variety of scenarios. However, they are susceptible to falling and leg malfunction during locomotion. Although the use of a large number of legs can overcome these problems, it makes the body long and leads to many legs being constrained to contact with the ground to support the long body, which impedes maneuverability. To improve the locomotion maneuverability of such robots, this study focuses on dynamic instability, which induces rapid and large movement changes, and uses a 12-legged robot with a flexible body axis. Our previous work found that the straight walk of the robot becomes unstable through a Hopf bifurcation when the body-axis flexibility is changed, which induces body undulations. Furthermore, we developed a simple controller based on the Hopf bifurcation and showed that the instability facilitates the turning of the robot. In this study, we newly found that the straight walk becomes unstable through a pitchfork bifurcation when the body-axis flexibility is changed in a way different from that in our previous work. In addition, the pitchfork bifurcation induces a transition into a curved walk, whose curvature can be controlled by the body-axis flexibility. We developed a simple controller based on the pitchfork bifurcation characteristics and demonstrated that the robot can perform a turning maneuver superior to that with the previous controller. This study provides a novel design principle

for maneuverable locomotion of many-legged robots using intrinsic dynamic properties.

**Index Terms**—Curved walk, instability, maneuverability, many-legged robot, pitchfork bifurcation, turning.

## I. INTRODUCTION

LEGGED locomotion, such as that of animals, allows excellent terrestrial mobility for traversing diverse environments. Legged robots, thus, have potential to be deployed in a wide variety of scenarios, such as search and rescue [21], [35], hazardous environment operation and exploration [9], [51], and planetary exploration [6], [55]. Various legged robots with agile animal-like locomotion have recently been developed [1], [4], [23]–[25], [30], [33], [36], [37], [40], [46]. However, most of these robots have four legs, and falling, which may result in the breakdown of mechanical and electrical components and from which it is difficult to recover, is inevitable during locomotion. Furthermore, damage to even one leg greatly degrades their locomotive performance [12]. The use of a large number of legs prevents falling and allows a certain level of leg malfunction to be tolerated [27], [34].

Although the use of a large number of legs has advantages for legged robots, it makes the body long and increases the difficulty of motion planning and control due to many intrinsic degrees of freedom and complex interaction with the environment. In particular, many legs are physically constrained to be in contact with the ground to support the long body, which can impede maneuverability. While humans and quadrupeds lean their bodies to enhance turning maneuvers, the underlying mechanism of agile locomotion using a large number of legs remains unclear from biological and engineering viewpoints [18]. Thus, maneuverable locomotion for robots with a large number of legs remains challenging.

Conventional controllers precisely plan the motion of all degrees of freedom of the robot (e.g., how the long body is bent, where each foot touches the ground, and in what order the legs move) and control the robot to stabilize the desired motion. However, this approach has huge computational and energy costs, making it inefficient. To design a simple and efficient controller with high locomotor performance, the fundamental dynamic principles embedded in the robot dynamics, including the interaction with the environment, should be fully utilized [1], [10], [29], [30].

Manuscript received 6 August 2021; revised 27 October 2021; accepted 4 January 2022. Date of publication 10 May 2022; date of current version 4 October 2022. This work was supported in part by the Japan Society for the Promotion of Science (JSPS) Grants-in-Aid for Scientific Research under Grants JP17H04914, JP19KK0377, JP19H04193, and JP20H00229, in part by the Japan Science and Technology Agency (JST) Fusion Oriented REsearch for disruptive Science and Technology (FOREST) Program under Grant JPMJFR2021, and in part by the Inamori Foundation. This article was recommended for publication by Associate Editor M. Fallon and Editor E. Yoshida upon evaluation of the reviewers' comments. (*Corresponding author: Shinya Aoi.*)

Shinya Aoi is with the Department of Mechanical Science and Bioengineering, Graduate School of Engineering Science, Osaka University, Osaka 560-8531, Japan (e-mail: aoi.shinya.es@osaka-u.ac.jp).

Ryoe Tomatsu, Yuki Yabuuchi, Daiki Morozumi, Kota Okamoto, Kei Senda, and Kazuo Tsuchiya are with the Department of Aeronautics and Astronautics, Graduate School of Engineering, Kyoto University, Kyoto 615-8540, Japan (e-mail: ryoe.tomatsu@gmail.com; elpistolero2125@gmail.com; morozumi.daiki.43a@st.kyoto-u.ac.jp; okamoto.kota.78z@st.kyoto-u.ac.jp; senda@kuaero.kyoto-u.ac.jp; tsuchiya\_k@nifty.com).

Soichiro Fujiki is with the Department of Physiology, School of Medicine, Dokkyo Medical University, Tochigi 321-0293, Japan (e-mail: sofujiki@gmail.com).

This article has two supplementary movies showing the pitchfork bifurcation of a straight walk (Movie 1) and turning performance (Movie 2) in the robot experiments. Contact Shinya Aoi (aoi.shinya.es@osaka-u.ac.jp) for further questions about this work.

This article has supplementary material provided by the authors and color versions of one or more figures available at <https://doi.org/10.1109/TRO.2022.3158194>.

Digital Object Identifier 10.1109/TRO.2022.3158194

For maneuverable locomotion of many-legged robots that overcomes the above difficulties and the limitations of conventional approaches, this study focuses on dynamic instability, which induces rapid and large movement changes, and uses a 12-legged robot whose body axis is flexible. Our previous work [2] showed that although many ground contact legs can impede maneuverability, they induce straight walk instability and body undulations through the Hopf bifurcation when the body-axis flexibility is changed; the bifurcation qualitatively changes a dynamical system by changing a parameter, and the Hopf bifurcation changes the stability of an equilibrium point and creates a limit cycle [47]. Stability refers to the capability to resist and recover from disturbances; the straight walk instability is, thus, expected to allow the robot to easily change walking direction. Therefore, we developed a simple controller based on the straight walk instability induced by the Hopf bifurcation to change the walking direction without precise motion planning and control and demonstrated that the straight walk instability facilitates the turning of the robot [3].

In this study, we show that the pitchfork bifurcation of the straight walk is caused by changes in the body-axis flexibility in a way different from that in the previous work [2], [3]; the pitchfork bifurcation changes the stability of an equilibrium point and creates two equilibrium points [47]. The pitchfork bifurcation not only destabilizes straight walking, but also causes curved walking, where the flexible body axis forms a curved shape. Furthermore, we found that the curvature of curved walking can be controlled by the body-axis flexibility. We developed a simple control strategy based on the pitchfork bifurcation characteristics, which improved the turning maneuver compared to that achieved using the Hopf bifurcation. This study also provides a design principle for a simple and efficient control scheme to create maneuverable locomotion for various robots using intrinsic dynamic properties.

## II. ROBOT

We used the many-legged robot developed in [2] and improved in [3]. The total length and mass are 135 cm and 8.5 kg, respectively. The robot consists of six body-segment modules (modules 1–6), as shown in Fig. 1. Each module is composed of a single body and one pair of legs and has the same length. The body segments are passively connected by yaw joints (yaw joints 1–5), in which torsional springs [the spring constant is  $k_i$  ( $i = 1, \dots, 5$ )] and potentiometers are installed at the axes. The yaw joint angles are zero when the body segments are aligned. Each leg has two links connected by pitch joints. The legs in the first module (module 1) have an additional link connected by a yaw joint to supplement the control of the walking direction during turning tasks. Each leg joint is manipulated by an encoder-equipped motor. The first module has a laser range scanner with a viewing angle of  $240^\circ$  (Hokuyo, URG-04LX) to find the relative position of a target for turning. The robot was controlled by an external host computer (Intel Pentium 4 2.8 GHz, RT-Linux) with 2-ms intervals and walked on a flat wooden floor with a vinyl floor mat to suppress slipping. The

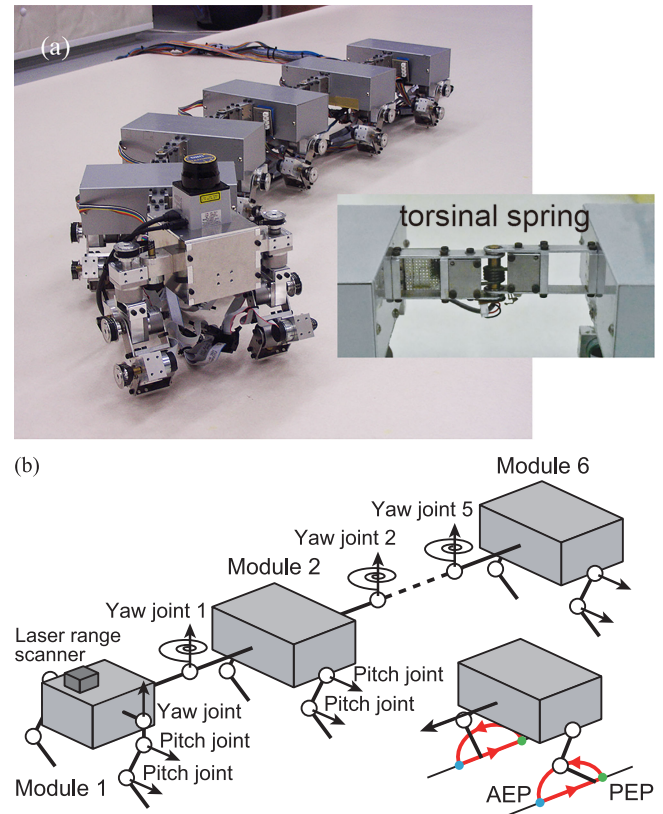


Fig. 1. (a) Photograph and (b) schematic model of the many-legged robot. The robot consists of six modules, each of which has one body segment and one pair of legs. The legs are controlled by two pitch joints so that the leg tips follow a periodic trajectory, including the AEP and the PEP. Body segments are passively connected by yaw joints with installed torsional springs. The legs in the first module have additional yaw joints to change the walking direction. A laser range scanner is installed on the first module to find a position relative to a target.

computer control signals and electric power were provided via external cables, which were kept slack and suspended to avoid influencing the locomotor behavior of the robot.

To make the robot walk in a straight line, we controlled the legs using the two pitch joints of each leg to follow the desired movement, which consists of two parts, namely, half of an elliptical curve that starts from the posterior extreme position (PEP) and ends at the anterior extreme position (AEP) and a straight line from the AEP to the PEP [see Fig. 1(b)]. In the straight line, the leg tips moved from the AEP to the PEP at a constant speed parallel to the body. We set the duration of the half elliptical curve to 0.29 s and that of the straight line to 0.31 s, and the distance between the AEP and the PEP in each leg is set to 3 cm. The left and right legs in each module moved in antiphase, and the relative phase between the ipsilateral legs on adjacent modules was set to  $2\pi/3$  rad. When the leg yaw joint angles of the first module were fixed so that the leg tip trajectories were parallel to the body, the robot was expected to walk in a straight line while keeping the body segments parallel to each other because torsional springs were installed on the body-segment yaw joints and all support-leg tips moved parallel to the body segments at an identical speed.

### III. PITCHFORK BIFURCATION OF STRAIGHT WALK

#### A. Experimental Results

Our previous work [2], [3] revealed that when we used torsional springs with the same spring constant for all the body-segment yaw joints (yaw joints 1–5) and changed the spring constant uniformly among the joints, the straight walk became unstable through the Hopf bifurcation, which induced body undulations. This bifurcation was verified by a Floquet analysis, which investigates the stability of solutions of linear differential equations with periodic coefficients, with a simple physical model. In this study, we performed robot experiments of walking in a straight line, where we changed the body-axis flexibility in a way that was different from that in our previous work. Specifically, we used the same torsional spring for yaw joints 2–5 with  $k_i = 41 \text{ N} \cdot \text{mm}^\circ$  ( $i = 2, \dots, 5$ ) and various torsional springs for yaw joint 1 with  $k_1 = 15, 17, 21, 28, 41$ , and  $75 \text{ N} \cdot \text{mm}^\circ$ . We set all the body segments parallel to each other as the initial conditions. The leg yaw joints in the first module were fixed during the experiments, and we did not attempt to control the walking direction, that is, the walking direction was an open loop.

When we used large spring constants for  $k_1$ , the robot kept walking in a straight line as expected, and the body segments were aligned, with all the body-segment yaw joint angles being almost zero [see Fig. 2(a) and (e) and Movie 1]. However, when  $k_1$  was set to below a threshold value, the body-segment yaw joints showed nonzero angles with the same sign, that is, the body axis was curved and the robot walked in a curved line [see Fig. 2(b), (f), and (g) and Movie 1]. Specifically, the robot walked in a curved line for  $k_1 = 15, 17, 21$ , and  $28 \text{ N} \cdot \text{mm}^\circ$ , but not for  $k_1 = 41$  and  $75 \text{ N} \cdot \text{mm}^\circ$ . Furthermore, both the left- and right-curved walking appeared. Fig. 2(c) shows the angles of yaw joint 1 for  $1/k_1$  averaged over 5 s during a curved walk (the angles for the other body-segment yaw joints are shown in Fig. 3). Although the angles slightly differ among yaw joints 1–5 partly due to feet slippage, these data indicate that the body axis shows a curved shape. Furthermore, while the fluctuation among the trials increases with  $1/k_1$ , the magnitude of these angles increases with  $1/k_1$ . These results suggest that the presence of the pitchfork bifurcation depends on  $k_1$ . These angle data were fitted by the square root of  $1/k_1$  [47]. The bifurcation point was estimated to be  $k_1 = 34 \text{ N} \cdot \text{mm}^\circ$  ( $1/k_1 = 0.030^\circ/\text{N} \cdot \text{mm}$ ).

The dependence of the body-segment yaw joint angles on  $1/k_1$  [see Figs. 2(c) and 3] indicates the change of the curved shape of the body axis for the curved walk. Fig. 2(d) shows the radius of curvature  $r$  of the body axis for  $1/k_1$  calculated as  $r = 5L / \sum_{i=1}^5 |\theta_i|$ , where  $\theta_i$  is the angle of yaw joint  $i$  ( $i = 1, \dots, 5$ ) and  $L$  is the length of the body segments. This figure shows that we can control the curvature of the body axis to perform a curved walk by adjusting  $k_1$  through the pitchfork bifurcation.

The pitchfork bifurcation also depends on parameters other than  $k_1$ . To investigate this, we used different values for the spring constant of yaw joints 2–5, gait speed, and relative phase between the ipsilateral legs on adjacent modules. Specifically, we changed  $k_{2-5}$  from 41 to  $28 \text{ N} \cdot \text{mm}^\circ$ , the distance between the AEP and the PEP in each leg [see Fig. 1(b)] from 3 to

1.8 cm, or the relative phase from  $2\pi/3$  to  $\pi$  and performed the same experiments shown in Fig. 2. As a result, these values also induced a curved walk below a critical value of  $k_1$ . However, the estimated bifurcation point and radius of curvature of the body axis changed, as shown in Fig. 4. Specifically, when the spring constant of yaw joints 2–5 and gait speed decreased, the estimated bifurcation point decreased from  $k_1 = 34$  to 23 and 25  $\text{N} \cdot \text{mm}^\circ$  ( $1/k_1 = 0.030$  to 0.043 and 0.040 $^\circ/\text{N} \cdot \text{mm}$ ), respectively. However, the radius of curvature remained almost unchanged. In contrast, while the relative phase did not change the bifurcation point as much ( $k_1 = 31 \text{ N} \cdot \text{mm}^\circ$ ,  $1/k_1 = 0.032^\circ/\text{N} \cdot \text{mm}$ ), it achieved a smaller radius of curvature.

#### B. Verification by the Floquet Analysis With a Simple Physical Model

The robot experiments suggested that the presence of the pitchfork bifurcation in the straight walk depends on the spring constant  $k_1$  [see Figs. 2(c), 3, and 4]. We verified this bifurcation from a theoretical viewpoint using a Floquet analysis with a simple physical model, as done in our previous work [2]. The model was simplified from the original high-dimensional mechanical model to extract the fundamentals of locomotion dynamics [see Fig. 5(a)]. In particular, the model was 2-D because the movements were designed to make the robot walk without up-and-down, roll, or pitch motions of the body segments. Furthermore, because an important role of legs in locomotion is to receive reaction forces from the floor, we neglected the inertial force of the legs and instead modeled the reaction forces at the leg tips based on the geometric conditions. Specifically, we assumed that the leg tips move relative to the body segments as designed and that the leg tips receive the friction forces during the straight line from the AEP to the PEP [see Fig. 1(b)], which are proportional to the velocities relative to the floor.

The equations of motion of the simple model can be expressed as

$$K(q)\ddot{q} + h(q, \dot{q}) = u(q, \dot{q}) + \lambda(q, \dot{q}, t) \quad (1)$$

where  $q = [x \ y \ \theta_0 \ \dots \ \theta_5]^\text{T}$ ,  $[x \ y]$  and  $\theta_0$  are the position and the yaw angle of the first module, respectively,  $K(q)$  is the inertia matrix,  $h(q, \dot{q})$  is the nonlinear term,  $u(q, \dot{q})$  is the torque term of the torsional springs, and  $\lambda(q, \dot{q}, t)$  is the reaction force term. Because the leg tips move periodically relative to the body segments, the reaction force  $\lambda$  becomes a function of time  $t$ . The detailed description and derivation of the equations of motion (1) are shown in our previous work [2]. During the straight walk of the model, we can write  $\hat{q} = [vt + x_0 \ y_0 \ 0 \ \dots \ 0]^\text{T}$  and  $\dot{\hat{q}} = [v \ 0 \ 0 \ \dots \ 0]^\text{T}$ , where  $x_0$  and  $y_0$  represent the initial position of the first module and  $v$  is the velocity of the leg tips relative to the body segments. For  $z^\text{T} = [q^\text{T} \ \dot{q}^\text{T}]$ , the linearization of the equations of motion (1) for a straight walk using  $z = \hat{z} + \delta z$  gives

$$\delta \dot{z} = A(t)\delta z. \quad (2)$$

Because the movements of the leg tips are periodic with the gait cycle  $\tau$ ,  $A(t + \tau) = A(t)$  is satisfied. The detailed description and derivation of the linearized equation (2) are also shown in

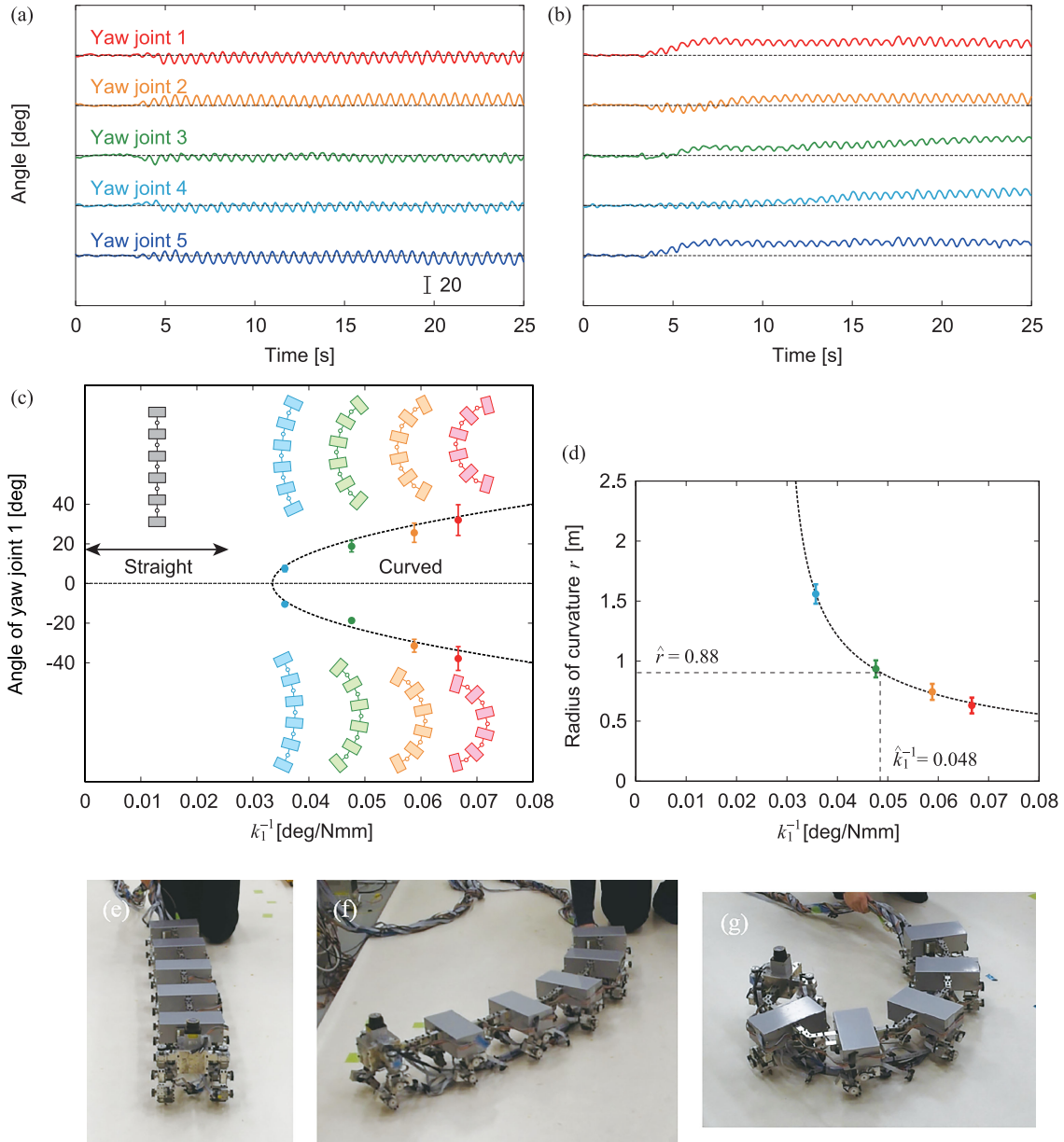


Fig. 2. Characteristics of the curved walk for  $k_1$  values below the threshold value. Yaw joint angles for (a) straight walk with  $k_1 = 41 \text{ N} \cdot \text{mm}^\circ$  and (b) curved walk with  $k_1 = 15 \text{ N} \cdot \text{mm}^\circ$  (see Movie 1). (c) Average angle of yaw joint 1 during the curved walk for  $1/k_1$  that indicates the pitchfork bifurcation. The data points and error bars correspond to the means and standard errors, respectively, of the results of five experiments. (d) Radius of curvature of body axis for  $1/k_1$ . The data points and error bars correspond to the means and standard errors, respectively, of the results of ten experiments. Photographs of (e) straight walk with  $k_1 > \hat{k}_1$ , (f) curved walk with small curvature with  $k_1 \sim \hat{k}_1$ , and (g) curved walk with large curvature with  $k_1 < \hat{k}_1$ .

our previous work [2]. The fundamental solution matrix  $Z(t)$  of the linearized equation with periodic coefficients (2) can be expressed as

$$Z(t) = \Phi(t)e^{\Lambda t} \quad (3)$$

where  $\Phi(t + \tau) = \Phi(t)$  [19]. Because we can use an identity matrix for  $Z(0)$  and  $\Phi(0)$ , the integration of (2) from  $t = 0$  to  $\tau$  yields

$$Z(\tau) = \Phi(\tau)e^{\Lambda\tau} = \Phi(0)e^{\Lambda\tau} = e^{\Lambda\tau}. \quad (4)$$

The Floquet exponents (eigenvalues of the constant matrix  $\Lambda$ ) and corresponding eigenvectors explain the behavior of the

model. Specifically, when all the real parts of the exponents are negative, the straight walk of the model is asymptotically stable. In contrast, if any real part of the exponents is positive, the straight walk becomes unstable. In our previous work [2], when all the spring constants of yaw joints 1–5 of the simple model were decreased uniformly, one pair of the Floquet exponents crossed the imaginary axis from the left-half plane and entered the right-half plane above a critical value of the spring constant, which indicates an oscillatory destabilization of the straight walk to produce body undulations and implied the Hopf bifurcation (strictly speaking, this corresponds to Neimark–Sacker bifurcation when considering the periodicity of the gait cycle [26]).

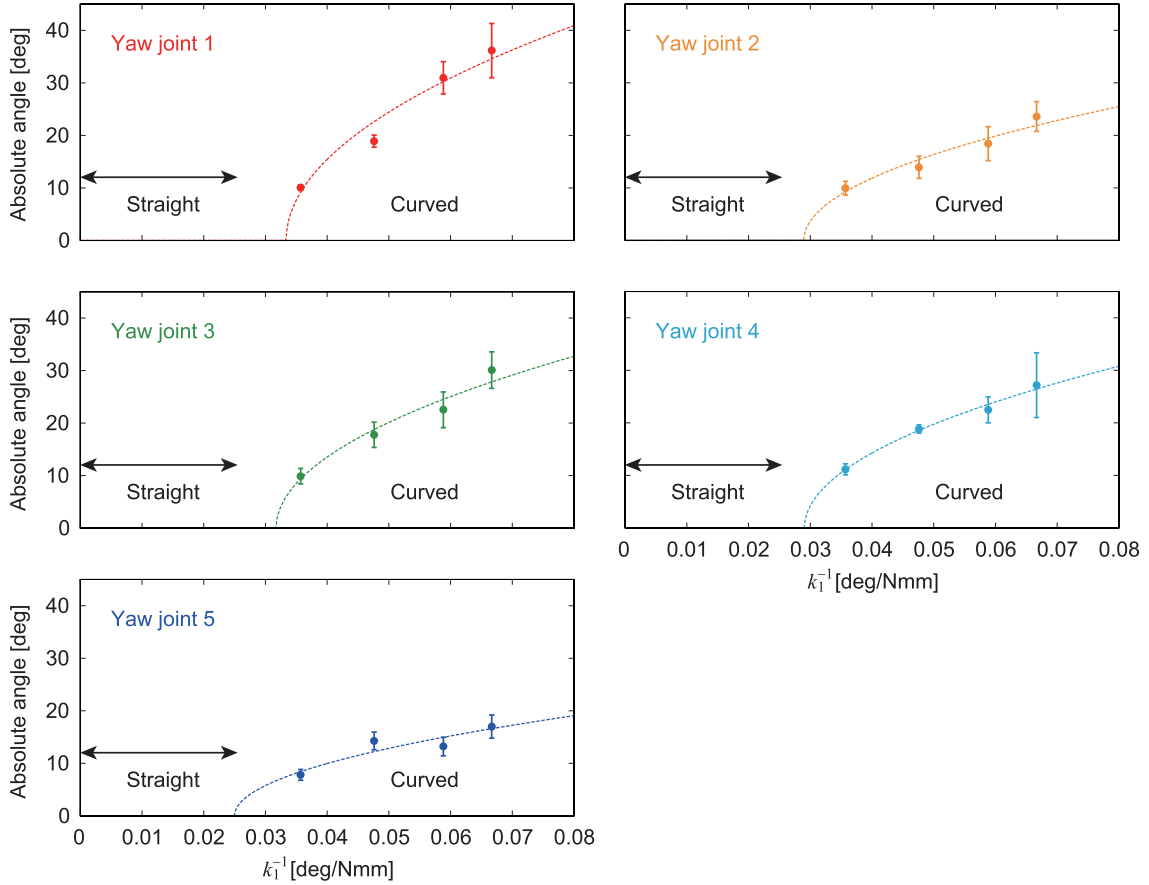


Fig. 3. Average absolute angles of body-segment yaw joints during the curved walk for  $1/k_1$ . The data points and error bars correspond to the means and standard errors, respectively, of the results of ten experiments.

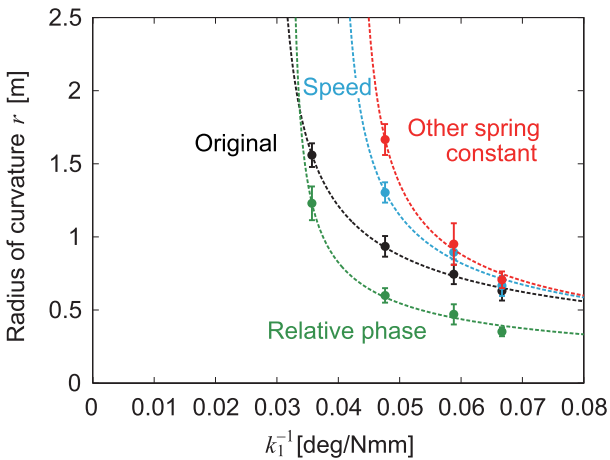


Fig. 4. Change in the radius of curvature by different values for the spring constant of yaw joints 2–5, gait speed, and relative phase between the ipsilateral legs on adjacent modules. The data points and error bars correspond to the means and standard errors, respectively, of the results of five experiments.

Furthermore, the relative amplitude and phase between the components of the destabilizing eigenvector were comparable to those of the yaw joint movements during the robot experiments. The Floquet analysis using a simple model is useful for verifying the bifurcation observed in the robot experiments.

Fig. 5(b) shows the Floquet exponents of the simple model when  $k_1$  was varied, while the other spring constants  $k_i$  ( $i = 2, \dots, 5$ ) remained fixed, as done in the robot experiments. Except for the zero exponents, all the exponents lie in the left-half plane for large  $k_1$ . However, with decreasing  $k_1$ , one exponent moves along the real axis and enters the right-half plane above  $k_1 = 12 \text{ N} \cdot \text{mm}/^\circ$ . Although this critical value is smaller than the bifurcation point estimated in the robot experiments in Section III-A, the components of the destabilizing eigenvector for yaw joints 1–5 at the critical point were 0.64, 0.36, 0.48, 0.46, and 0.16, respectively, showing the same sign. This indicates that the straight walk is destabilized to produce a curved walk (positive disturbance induces a right-curved walk and negative disturbance induces a left-curved walk) and implies the pitchfork bifurcation. Furthermore, the ratio between the components of the destabilizing eigenvector is consistent with the ratio between the yaw joint angles during the curved walk of the robot experiments (see Fig. 3). Although this analysis does not estimate the radius of curvature after the bifurcation due to the limitation of the linear analysis, these results verify the destabilization of the straight walk and the emergence of a curved walk through the pitchfork bifurcation, as observed in the robot experiments.

We also investigated the parameter dependence of the pitchfork bifurcation. Fig. 5(c) shows how the critical value of  $k_1$  changes as the spring constant of yaw joints 2–5, gait speed, and

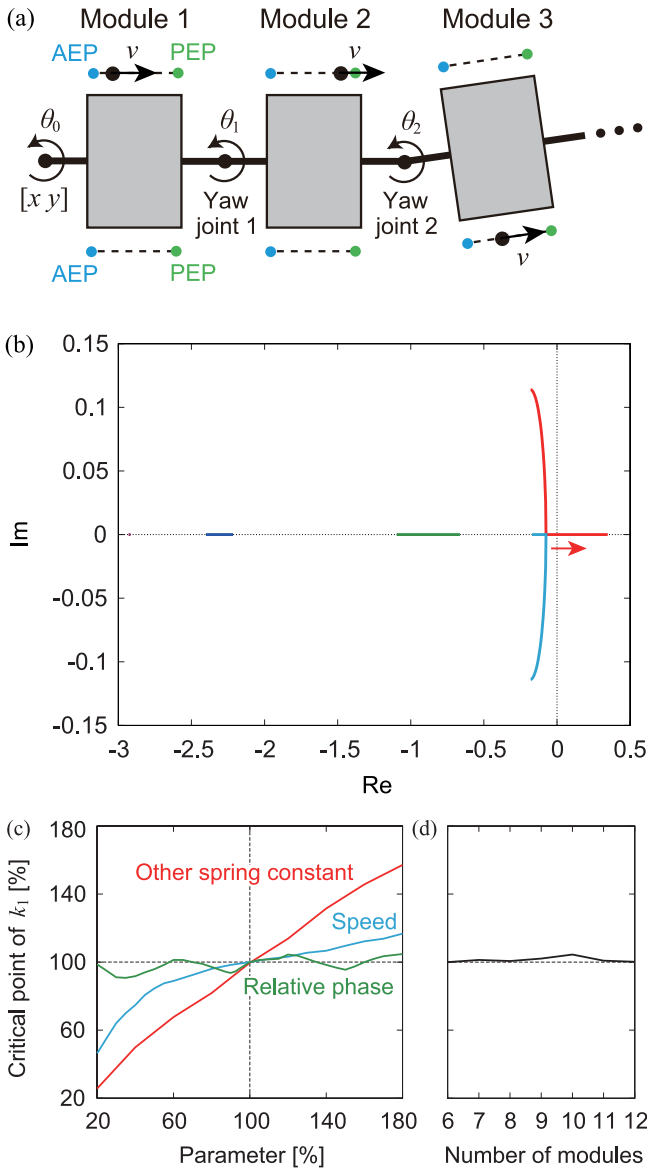


Fig. 5. Floquet analysis using a simple 2-D model. (a) Simple model. (b) Floquet exponents when  $k_1$  was varied. Different colors represent different exponents. The exponent in red crosses into the right-half plane along the real axis, indicating the pitchfork bifurcation. The change in the critical value of  $k_1$  by (c) spring constant of yaw joints 2–5, gait speed, and relative phase between the ipsilateral legs on adjacent modules, and (d) number of modules.

relative phase between the ipsilateral legs on adjacent modules change in the same way as in the robot experiments in Fig. 4. In addition, Fig. 5(d) shows the change in the critical value when the number of body segments is increased. When the spring constant of yaw joints 2–5 and the gait speed decrease, the critical value decreases. However, the relative phase does not change the critical value as much. These results are consistent with those in the robot experiments (see Fig. 4). The number of body segments also does not change the critical value very much. Although we investigated the effects of only changes in the spring constant of yaw joints 2–5, gait speed, relative phase, and the number of body segments, this Floquet analysis can

investigate other parameters, such as the length and the mass, as performed in our previous work [2] for the Hopf bifurcation.

#### IV. TURNING MANEUVERABILITY

##### A. Turning Strategy Based on the Pitchfork Bifurcation

To investigate the maneuverability of the robot achieved with the aid of the pitchfork bifurcation, we focused on a turning task in which the robot approached a target located on the floor in a direction different from that to which the robot was oriented, as performed in our previous work [3], which investigated the maneuverability with the aid of the Hopf bifurcation. For a target at any location (relative angle  $\psi$  and distance  $R$ ), there exists a unique radius of curvature  $\hat{r}$  of the curved walk with which the robot will approach the target [see Fig. 6(a)]. Because the radius of curvature  $r$  of the body axis induced by the pitchfork bifurcation monotonically decreases with  $1/k_1$  [see Fig. 2(d)],  $k_1 = \hat{k}_1$  is uniquely determined so that  $r = \hat{r}$ . This means that when we use  $k_1 = \hat{k}_1$ , the robot spontaneously approaches the target due to the pitchfork bifurcation characteristics, which is an optimal strategy for turning. However, this strategy is feedforward, depending on the initial conditions of the robot and the target, that is, an open loop for the walking direction. In particular, the direction in which the robot turns (left or right) depends on the initial robot conditions because of the pitchfork bifurcation characteristics, and thus, this strategy does not guarantee the success of the turning tasks. Therefore, we also used a supplementary turning controller developed in our previous work [3], which uses the laser range scanner of the first module to measure the relative target angle and manipulates the leg yaw joints of the first module to approach the target based on the measured target angle (see the Appendix). This supplementary controller is a closed loop for the walking direction and allows the robot to approach the target even when  $k_1 \neq \hat{k}_1$ .

##### B. Experimental Results

For the initial conditions, we used  $\psi = 45^\circ$  and  $R = 1.3$  m for the relative angle and the distance between the first module and the target, respectively, which yielded  $\hat{r} = 0.88$  m and  $\hat{k}_1 = 21$  N · mm/ $^\circ$  ( $1/\hat{k}_1 = 0.048^\circ/\text{N} \cdot \text{mm}$ ), and set all the body-segment yaw joint angles to zero [see Fig. 6(f)]. Fig. 6(b) shows the trajectory of the first module on the floor during the turning task for three torsional spring constants, namely,  $k_1 = 15$  ( $< \hat{k}_1$ ),  $21$  ( $\sim \hat{k}_1$ ), and  $41$  N · mm/ $^\circ$  ( $> \hat{k}_1$ ). Fig. 6(c) and (d) shows the time profiles of the target distance and the relative target angle with respect to the walking direction, respectively, for these three spring constants. When the distance was less than 0.15 m, we assumed that the robot reached the target, and this task was successfully completed. For  $k_1 = 41$  N · mm/ $^\circ$  ( $> \hat{k}_1$ ), the robot hardly changed the walking direction, and the first module trajectory bulged outward. As a result, the robot could not reach the target [see Fig. 6(g) and Movie 2]. For  $k_1 = 15$  N · mm/ $^\circ$  ( $< \hat{k}_1$ ), although the robot could quickly change the walking direction, it moved in directions away from the target due to the small radius of curvature created by the

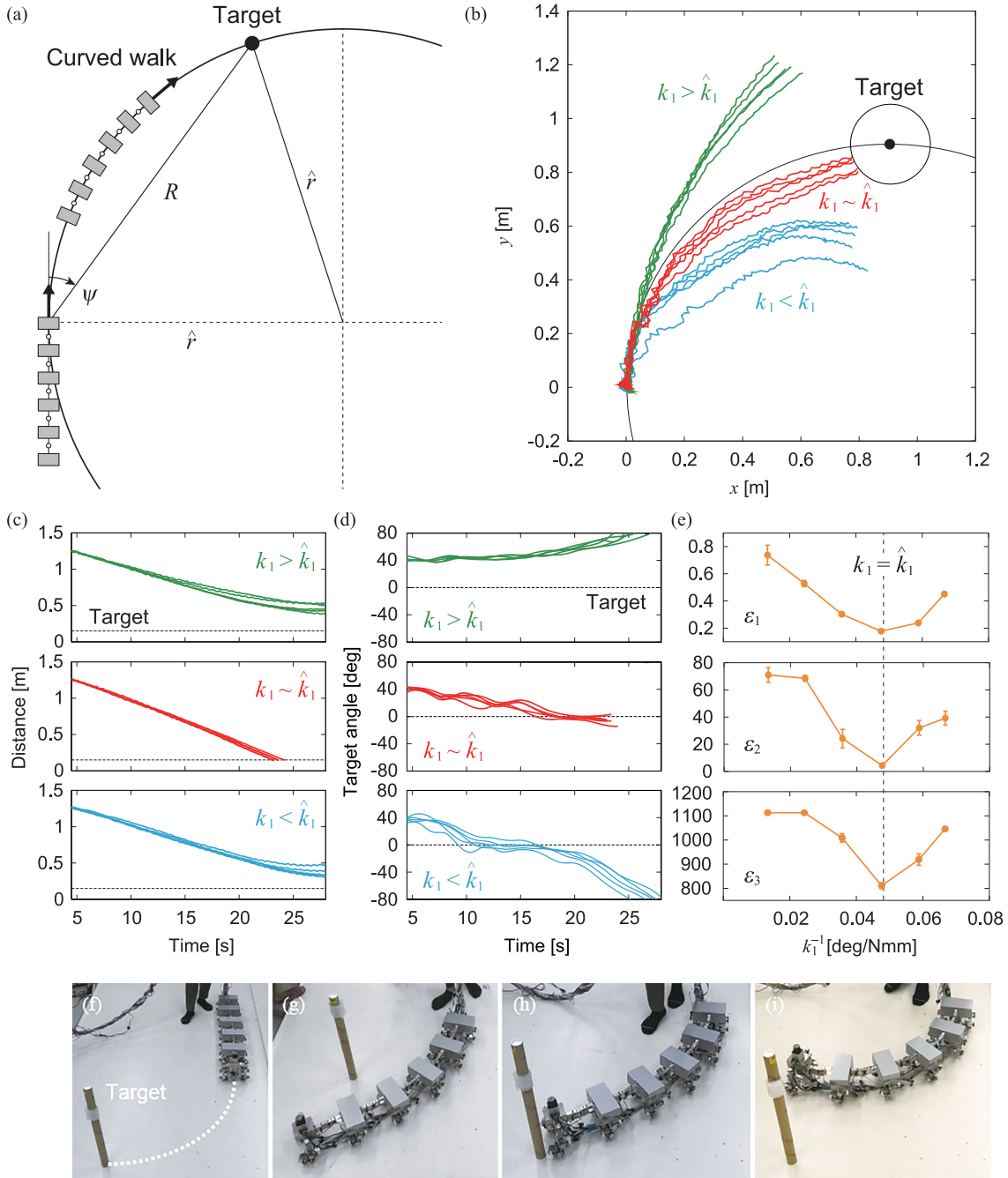


Fig. 6. Turning task. (a) Radius of curvature  $\hat{r}$  of the curved walk with which the robot approaches a target (relative angle  $\psi$  and distance  $R$ ). (b) Trajectory of the first module on the floor, (c) target distance, and (d) relative target angle for five experiments for three spring constants with  $\psi = 45^\circ$ ,  $R = 1.3$  m,  $\hat{r} = 0.88$  m, and  $1/\hat{k}_1 = 0.048^\circ/\text{N} \cdot \text{mm}$  (see Movie 2). (e) Evaluation criteria  $\varepsilon_1$ ,  $\varepsilon_2$ , and  $\varepsilon_3$  for  $1/k_1$ . The data points and error bars correspond to the means and standard errors, respectively, of the results of five experiments. Photographs of (f) initial conditions, (g) unsuccessful approach with  $k_1 > \hat{k}_1$ , (h) successful approach with  $k_1 \sim \hat{k}_1$ , and (i) unsuccessful approach with  $k_1 < \hat{k}_1$ .

pitchfork bifurcation and could not reach the target [see Fig. 6(i) and Movie 2]. In contrast, for  $k_1 = 21 \text{ N} \cdot \text{mm}^\circ$  ( $\sim \hat{k}_1$ ), the robot reached the target through the optimal curved walk generated by the pitchfork bifurcation [see Fig. 6(h) and Movie 2].

To quantitatively clarify the turning performance dependence on  $k_1$ , we employed three evaluation criteria, namely,  $\varepsilon_1$ ,  $\varepsilon_2$ , and  $\varepsilon_3$ . For criterion  $\varepsilon_1$ , we used the distance of the target at 23 s (the earliest time at which the task is successfully completed)

to evaluate how quickly and successfully the robot approached the target. For criterion  $\varepsilon_2$ , we used the absolute value of the relative target angle with respect to the walking direction at 23 s to evaluate how quickly and successfully the robot was oriented to the target. For criterion  $\varepsilon_3$ , we used the amount of the control input during the task from the supplementary turning control in the leg yaw joints of the first module (see the Appendix) to evaluate how efficiently the robot performs turning. Specifically,

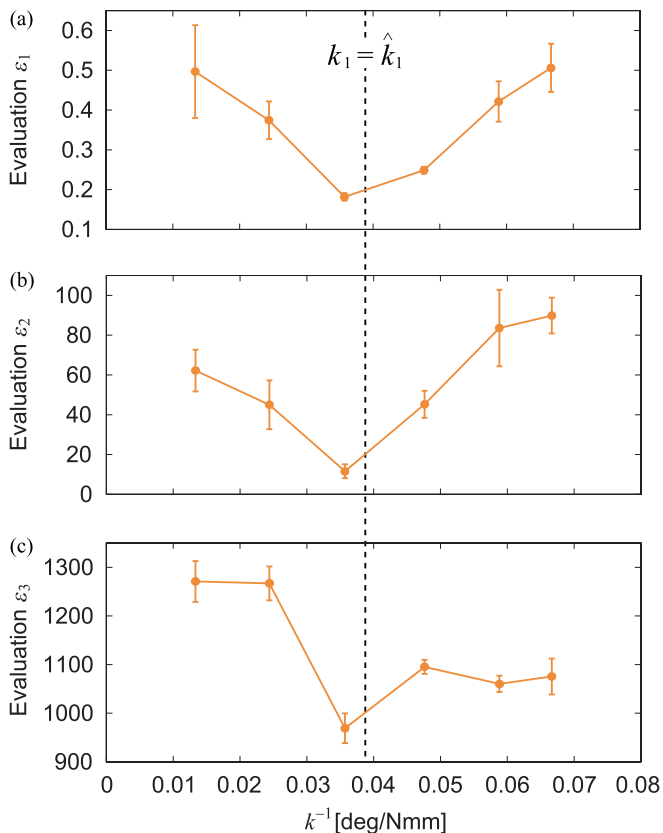


Fig. 7. Evaluation criteria (a)  $\varepsilon_1$ , (b)  $\varepsilon_2$ , and (c)  $\varepsilon_3$  for  $1/k_1$  for different conditions ( $1/\hat{k}_1 = 0.039^\circ/\text{N} \cdot \text{mm}$ ). The data points and error bars correspond to the means and standard errors, respectively, of the results of five experiments.

$\varepsilon_3 = \int (\hat{\psi}_1^2 + \hat{\psi}_2^2) dt$ . Fig. 6(e) shows the results for  $1/k_1$ . All the criteria showed minimum values around  $k_1 = \hat{k}_1$ , which means that the turning strategy using the pitchfork bifurcation achieved the best performance and that the robot made the best use of the curved walk induced by the pitchfork bifurcation to complete the turning task.

To verify the performance of the proposed controller using the pitchfork bifurcation, we additionally performed the same experiment as that in Fig. 6(b) but using the different initial conditions of the target, namely,  $\psi = 40^\circ$  and  $R = 1.5$  m, which yielded  $\hat{r} = 1.2$  m and  $\hat{k}_1 = 26 \text{ N} \cdot \text{mm}^\circ$  ( $1/\hat{k}_1 = 0.039^\circ/\text{N} \cdot \text{mm}$ ). Fig. 7(a)–(c) shows evaluation criteria  $\varepsilon_1$ ,  $\varepsilon_2$ , and  $\varepsilon_3$ , respectively, for  $1/k_1$ . All the criteria show minimum values around  $k_1 = \hat{k}_1$ , which means that the turning strategy using the pitchfork bifurcation achieved the best performance, in the same way as shown in Fig. 6(e). The results show similar trends, which verify the performance of the proposed controller.

### C. Contribution of Supplementary Turning Control

As demonstrated above, the robot achieved maneuverable and efficient turning to approach a target using the curved walk induced by the pitchfork bifurcation. However, when the robot starts the approach with the body axis straight, it takes some time for the convergence to a curved walk, as shown in Fig. 2(b). In addition, because the initial straight walk corresponds to

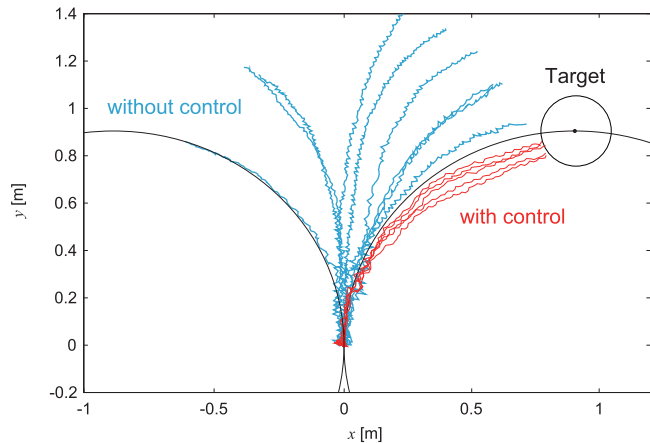


Fig. 8. Comparison of the trajectory of the first module on the floor during the turning task with and without the supplementary turning controller. Nine trials without the supplementary controller and five trials with the controller [see Fig. 6(b)] are shown.

the unstable solution of the pitchfork bifurcation, it is unclear whether the robot will turn to the left or the right, as shown in Fig. 2(c) (the disturbance determines the turning direction and the robot continues walking straight unless disturbed). Because the use of the optimal spring constant  $\hat{k}_1$  does not necessarily guarantee the success of the approach to the target, we also used the supplementary turning controller in the leg yaw joints in the first module.

To clarify the contribution of this supplementary controller, we also performed experiments without using the supplementary controller for  $k_1 = 21 \text{ N} \cdot \text{mm}^\circ$  ( $\sim \hat{k}_1$ ). The experimental conditions were identical to those in Fig. 6(b). Fig. 8 compares the trajectory of the first module on the floor during the turning task with and without the supplementary controller. In all the trials with the supplementary controller, the robot successfully approached the target. In contrast, the robot without the supplementary controller failed in many trials, because the robot started walking in a straight line and took some time to converge to walking in a curved line, and it sometimes curved to the different direction from the target, as expected.

### D. Comparison With the Previous Strategy

To examine how the turning performance was improved by the pitchfork bifurcation, we also performed experiments using the turning strategy based on the Hopf bifurcation used in our previous work [3] and compared the performance. For the Hopf bifurcation, we used the same spring constant among the body-segment yaw joints and employed five spring constants ( $k_i = 8.7, 11, 15, 21, \text{ and } 41 \text{ N} \cdot \text{mm}^\circ$ ,  $i = 1, \dots, 5$ ) to evaluate the turning performance for  $k_i$ , where the Hopf bifurcation point is about  $k_i = 18 \text{ N} \cdot \text{mm}^\circ$  ( $1/\hat{k}_i = 0.057^\circ/\text{N} \cdot \text{mm}$ ), as obtained in our previous work [3]. The experimental conditions were identical to those in Fig. 6(e) except for the spring constants of the body-segment yaw joints. Fig. 9(a)–(c) compares the turning performance in terms of criteria  $\varepsilon_1$ ,  $\varepsilon_2$ , and  $\varepsilon_3$ , respectively, between the strategies based on pitchfork and Hopf bifurcations. All the criteria for the Hopf bifurcation showed minimum values



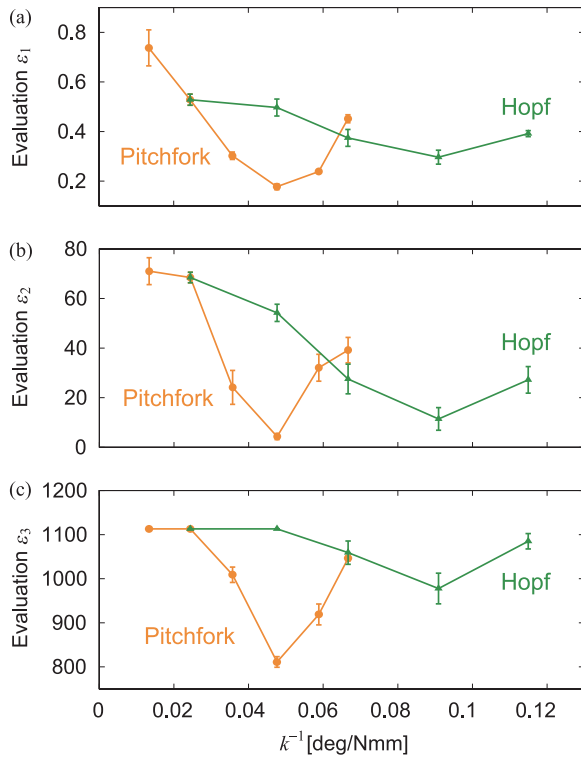


Fig. 9. Comparison of evaluation criteria (a)  $\varepsilon_1$ , (b)  $\varepsilon_2$ , and (c)  $\varepsilon_3$  between the turning strategies based on the pitchfork bifurcation and the Hopf bifurcation. The data points and error bars correspond to the means and standard errors, respectively, of the results of five experiments.

in the unstable region, as observed in our previous work [3]. However, the minimum values of the pitchfork bifurcation are lower than those of the Hopf bifurcation for all criteria. This means that the turning strategy based on the pitchfork bifurcation created by tuning the body-axis flexibility is superior to that based on the Hopf bifurcation, which was developed in our previous work [3].

## V. CONCLUSION

In this study, we found that the straight walk of a many-legged robot with flexible body axis becomes unstable through the pitchfork bifurcation when the body-axis flexibility is changed. The straight walk transitioned into the curved walk, whose curvature depended on the body-axis flexibility. We developed a simple controller based on the pitchfork bifurcation characteristics and demonstrated that the robot achieves high turning maneuver superior to the previous controller based on the Hopf bifurcation.

Maneuverability is related to the ability to change the movement direction. When the movement direction is destabilized during locomotion, the instability provides driving forces to rapidly change the movement direction and, thus, enhances maneuverability. Some military aircraft, such as the F-16, are designed to be aerodynamically unstable to enhance maneuverability [8], [28]. The use of dynamic instability is, thus, useful from an engineering viewpoint.

The strategy of using movement direction instability to enhance maneuverability is also used by animals. Because the instability is determined by the body dynamics during interaction with the environment, it is prominent in locomotion generated through aerodynamics and hydrodynamics, such as the locomotion of flying insects [15], [38], [49] and sea animals [16], [17], [53]. It also appears in legged locomotion. When the center of mass is high, as in mammals whose legs are under the body, leaning the body to the left or the right induces instability and helps turning [11], [42]. However, when the center of mass is low, as in reptiles and arthropods whose legs are away from the side of the body, locomotor behavior is almost 2-D because the center of mass moves in a horizontal plane. Therefore, the effect of body leaning is small, and thus, such a turning strategy cannot be used, which implies that the stability of the walking direction in the horizontal plane becomes more crucial. It has been suggested that cockroaches manipulate the position of the reaction forces from the floor entering the body to control the stability of a straight walk in a horizontal plane and that the straight walk instability helps their turning [39], [42].

Various bioinspired robots that use their body axis for propulsion, such as snake robots [7], [45] and fish robots [13], [31], [43], have high maneuverability. However, legged robots still have difficulty in achieving highly maneuverable locomotion. This is partly because their interaction with the environment (i.e., foot contact with the ground) is intermittent due to the repetition of foot-contact and foot-off phases in leg movement. Although this intermittency allows the traversal of diverse environments, it can make the robot lose balance. Therefore, the control design of legged robots has focused on the avoidance of balance loss using dynamic criteria, such as a supporting polygon [20] and a zero-moment point [52], and maneuverability has not been well investigated. Although increasing the number of legs prevents balance loss, it also increases the number of contact legs, which impedes maneuverability. Moreover, the number of degrees of freedom to be controlled increases, making both the motion planning and control difficult. In addition, many-legged robots generally use actuators for controlling not only the leg joints but also body-segment joints [48], [54], which requires huge computational and energy costs. In contrast, our robot has passive body-segment joints, which do not directly control the movement of the body axis, and instead determines the body-axis flexibility to induce a curved walk by the pitchfork bifurcation in the robot dynamics. The generation of robot movements with dynamics rather than actuators is crucial for efficient locomotion [10], and our strategy greatly reduces the computational and energy costs. Both the pitchfork and Hopf bifurcations induce the straight walk instability and, thus, contribute to the maneuverability. However, because the pitchfork bifurcation causes a curved walk used for turning, unlike the Hopf bifurcation that causes body undulations, the pitchfork bifurcation makes a greater contribution. Furthermore, when such bifurcation is introduced into the locomotion dynamics of other robots, such as snake and fish robots, through the mechanical and control design, it would contribute to improving their maneuverability.

In this study, we investigated the contribution of the pitchfork bifurcation to maneuverability in robot experiments, where the

robot performs turning only once on a flat floor. It is important to clarify the contribution of the pitchfork bifurcation in more complex scenarios and environments in the future. In particular, consecutive turnings are crucial for complex scenarios. However, when we consider the experiments where the robot sequentially approaches multiple targets placed at different locations on the floor, that is, the robot performs multiple consecutive turnings, the initial conditions of the targets, such as the relative angle and the distance, will differ in each turning. The different initial conditions of the targets induce the different radiuses of curvature for optimal turning, which require different body-axis flexibilities. Because our robot uses torsional springs to determine the body-axis flexibility, it is impossible to change the flexibility during the experiment. In future studies, we would like to improve our robot and controller, for example, by incorporating a variable flexibility mechanism in the body axis to conduct more complex tasks. In addition, various turning strategies have been developed in quadruped and hexapod robots to modulate the leg movements for turning using bioinspired approaches based on central pattern generators, sensory systems [5], [22], [32], [44], [50], [57], and optimization techniques [14], [41], [56]. We would like to improve our instability-based strategy in the body-axis movement based on these strategies to enhance the turning maneuverability of multilegged robots in the future.

## APPENDIX

### SUPPLEMENTARY TURNING CONTROL BY LEG JOINTS

The optimal turning strategy is feedforward, depending only on the initial relative position between the robot and the target. In addition, the direction in which the robot turns (left or right) depends on the initial robot conditions because of the property of the pitchfork bifurcation. To guarantee a successful approach to the target, we used a supplementary feedback-based turning controller, which was developed in our previous work [3]. Specifically, we used the relative target angle  $\psi$  of the first module measured by the laser range scanner and the leg yaw joints  $\psi_1$  and  $\psi_2$  of the first module. We determined the desired angles  $\hat{\psi}_1$  and  $\hat{\psi}_2$  of  $\psi_1$  and  $\psi_2$  for each gait cycle  $[t_i^n \leq t < t_i^n + T]$ , where  $t = t_i^n$  is the time when the desired leg tip is at the PEP for the  $n$ th gait cycle and  $T$  is the gait cycle duration ( $= 0.6$  s)] using

$$\hat{\psi}_i(t) = \begin{cases} \hat{\psi}_i(t_i^n), & t_i^n \leq t < t_i^n + t_{\text{start}} \\ \hat{\psi}_i(t_i^n) + \Delta_i \frac{t - t_i^n - t_{\text{start}}}{t_{\text{end}} - t_{\text{start}}}, & t_i^n + t_{\text{start}} \leq t \leq t_i^n + t_{\text{end}} \\ \hat{\psi}_i(t_i^n + t_{\text{end}}), & t_i^n + t_{\text{end}} < t < t_i^n + T \end{cases}$$

$$\Delta_i = \begin{cases} \psi(t_i^n + t_{\text{start}}) - \hat{\psi}_i(t_i^n + t_{\text{start}}), & |\psi(t_i^n + t_{\text{start}}) - \hat{\psi}_i(t_i^n + t_{\text{start}})| < 5^\circ \\ 5^\circ, & \text{otherwise} \end{cases}$$

where  $t_{\text{start}}$  and  $t_{\text{end}}$  were set to 40% and 80%, respectively, of the duration of the half elliptical curve of the leg tip trajectory ( $= 0.12$  and  $0.23$  s) determined experimentally. This controller means that each leg changed its yaw direction toward the target only during the swing phase with  $5^\circ$  of the maximum turning angle for one gait cycle. We also limited the maximum angle of

the leg yaw joint to  $5^\circ$  during the turning task. This supplementary control did not aim to make the robot follow the optimal curved path generated by the turning strategy using the pitchfork bifurcation. Instead, it was designed so that the first module modulated the walking direction based on the target direction, which solves the problems related to the feedforward property of the optimal turning strategies and the turning direction due to initial robot conditions and, furthermore, allows the robot to approach the target even when  $k_1 \neq \hat{k}_1$ .

## REFERENCES

- [1] J. Aguilar *et al.*, "A review on locomotion robotics: The study of movement at the intersection of robotics, soft matter and dynamical systems," *Rep. Prog. Phys.*, vol. 79, 2016, Art. no. 110001.
- [2] S. Aoi, Y. Egi, and K. Tsuchiya, "Instability-based mechanism for body undulations in centipede locomotion," *Phys. Rev. E*, vol. 87, 2013, Art. no. 012717.
- [3] S. Aoi, T. Tanaka, S. Fujiki, T. Funato, K. Senda, and K. Tsuchiya, "Advantage of straight walk instability in turning maneuver of multilegged locomotion: A robotics approach," *Sci. Rep.*, vol. 6, 2016, Art. no. 30199.
- [4] S. Aoi, P. Manoonpong, Y. Ambe, M. Matsuno, and F. Wörgötter, "Adaptive control strategies for interlimb coordination in legged robots: A review," *Front. Neurobot.*, vol. 11, 2017, Art. no. 39.
- [5] E. Arena, P. Arena, and L. Patanè, "Efficient hexapodal locomotion control based on flow-invariant subspaces," in *Proc. IFAC World Congr.*, 2011, pp. 13758–13763.
- [6] P. Arm *et al.*, "SpaceBok: A dynamic legged robot for space exploration," in *Proc. IEEE Int. Conf. Robot. Autom.*, 2019, pp. 6288–6294.
- [7] H. C. Astley *et al.*, "Modulation of orthogonal body waves enables high maneuverability in sidewinding locomotion," *Proc. Nat. Acad. Sci. USA*, vol. 112, pp. 6200–6205, 2015.
- [8] G. Avanzini and G. de Matteis, "Bifurcation analysis of a highly augmented aircraft model," *J. Guid., Control, Dyn.*, vol. 20, pp. 754–759, 1997.
- [9] J. S. Byrd and K. R. DeVries, "A six-legged telerobot for nuclear applications development," *Int. J. Robot. Res.*, vol. 9, pp. 43–52, 1990.
- [10] S. H. Collins, A. L. Ruina, R. Tedrake, and M. Wisse, "Efficient bipedal robots based on passive-dynamic walkers," *Science*, vol. 307, pp. 1082–1085, 2005.
- [11] G. Courtine and M. Schieppati, "Human walking along a curved path. II. Gait features and EMG patterns," *Eur. J. Neurosci.*, vol. 18, pp. 191–205, 2003.
- [12] A. Cully, J. Clune, D. Tarapore, and J.-B. Mouret, "Robots that can adapt like animals," *Nature*, vol. 521, pp. 503–507, 2015.
- [13] O. M. Curet, N. A. Patankar, G. V. Lauder, and M. A. MacIver, "Aquatic maneuvering with counter-propagating waves: A novel locomotive strategy," *J. Roy. Soc. Interface*, vol. 8, pp. 1041–1050, 2011.
- [14] J. Degraeve, M. Burm, T. Waegeman, F. Wyffels, and B. Schrauwen, "Comparing trotting and turning strategies on the quadrupedal oncilla robot," in *Proc. IEEE Int. Conf. Robot. Biomimetics*, 2013, pp. 228–233.
- [15] M. H. Dickinson, C. T. Farley, R. J. Full, M. A. R. Koehl, R. Kram, and S. Lehman, "How animals move: An integrative view," *Science*, vol. 288, pp. 100–106, 2000.
- [16] F. E. Fish, J. Hurley, and D. P. Costa, "Maneuverability by the sea lion *Zalophus californianus*: Turning performance of an unstable body design," *J. Exp. Biol.*, vol. 206, pp. 667–674, 2003.
- [17] F. E. Fish, "Balancing requirements for stability and maneuverability in cetaceans," *Integr. Comp. Biol.*, vol. 42, pp. 85–93, 2002.
- [18] R. J. Full, T. Kubow, J. Schmitt, P. Holmes, and D. Koditschek, "Quantifying dynamic stability and maneuverability in legged locomotion," *Integr. Comp. Biol.*, vol. 42, pp. 149–157, 2002.
- [19] J. Guckenheimer and P. Holmes, *Nonlinear Oscillations, Dynamical Systems, and Bifurcations of Vector Fields*. New York, NY, USA: Springer-Verlag, 2002.
- [20] S. A. Hirose, "Study of design and control of a quadruped walking vehicle," *Int. J. Robot. Res.*, vol. 3, pp. 113–133, 1984.
- [21] K. L. Hoffman and R. J. Wood, "Myriapod-like ambulation of a segmented microrobot," *Auton. Robot.*, vol. 31, pp. 103–114, 2011.
- [22] T. Horvat, K. Melo, and A. J. Ijspeert, "Spine controller for a sprawling posture robot," *IEEE Robot. Autom. Lett.*, vol. 2, no. 2, pp. 1195–1202, Apr. 2017.

- [23] J. Hwangbo *et al.*, “Learning agile and dynamic motor skills for legged robots,” *Sci. Robot.*, vol. 4, 2019, Art. no. eaa5872.
- [24] A. J. Ijspeert, A. Crespi, D. Ryczko, and J.-M. Cabelguen, “From swimming to walking with a salamander robot driven by a spinal cord model,” *Science*, vol. 315, pp. 1416–1420, 2007.
- [25] A. J. Ijspeert, “Biorobotics: Using robots to emulate and investigate agile locomotion,” *Science*, vol. 346, pp. 196–203, 2014.
- [26] Y. A. Kuznetsov, *Elements of Applied Bifurcation Theory*. New York, NY, USA: Springer-Verlag, 2004.
- [27] T. Kano, K. Sakai, K. Yasui, D. Owaki, and A. Ishiguro, “Decentralized control mechanism underlying interlimb coordination of millipedes,” *Bioinspiration Biomimetics*, vol. 12, 2017, Art. no. 036007.
- [28] H. G. Kwatny, W. H. Bennett, and J. Berg, “Regulation of relaxed static stability aircraft,” *IEEE Trans. Autom. Control*, vol. 36, no. 11, pp. 1315–1332, Nov. 1991.
- [29] C. Li, P. B. Umbanhowar, H. Komsuoglu, D. E. Koditschek, and D. I. Goldman, “Sensitive dependence of the motion of a legged robot on granular media,” *Proc. Nat. Acad. Sci. USA*, vol. 106, pp. 3029–3034, 2009.
- [30] C. Li, T. Zhang, and D. I. Goldman, “A terradynamics of legged locomotion on granular media,” *Science*, vol. 339, pp. 1408–1411, 2013.
- [31] R. D. Maladen, Y. Ding, P. B. Umbanhowar, A. Kamor, and D. I. Goldman, “Mechanical models of sandfish locomotion reveal principles of high performance subsurface sand-swimming,” *J. Roy. Soc. Interface*, vol. 8, pp. 1332–1345, 2011.
- [32] P. Manoonpong, U. Parlitz, and F. Wörgötter, “Neural control and adaptive neural forward models for insect-like, energy-efficient, and adaptable locomotion of walking machines,” *Front. Neural Circuits*, vol. 7, 2013, Art. no. 12.
- [33] C. Mastalli, I. Havoutis, M. Focchi, D. G. Caldwell, and C. Semini, “Motion planning for quadrupedal locomotion: Coupled planning, terrain mapping and whole-body control,” *IEEE Trans. Robot.*, vol. 36, no. 6, pp. 1635–1648, Dec. 2020.
- [34] A. Miguel-Blanco and P. Manoonpong, “General distributed neural control and sensory adaptation for self-organized locomotion and fast adaptation to damage of walking robots,” *Front. Neural Circuits*, vol. 14, 2020, Art. no. 46.
- [35] M. Ning *et al.*, “Design and analysis for a multifunctional rescue robot with four-bar wheel-legged structure,” *Adv. Mech. Eng.*, vol. 10, pp. 1–14, 2018.
- [36] D. Owaki and A. Ishiguro, “A quadruped robot exhibiting spontaneous gait transitions from walking to trotting to galloping,” *Sci. Rep.*, vol. 7, 2017, Art. no. 277.
- [37] H.-W. Park, P. M. Wensing, and S. Kim, “High-speed bounding with the MIT Cheetah 2: Control design and experiments,” *Int. J. Robot. Res.*, vol. 36, pp. 167–192, 2017.
- [38] M. M. Parsons, H. G. Krapp, and S. B. Laughlin, “Sensor fusion in identified visual interneurons,” *Curr. Biol.*, vol. 20, pp. 624–628, 2010.
- [39] J. Proctor and P. Holmes, “Steering by transient destabilization in piecewise-holonomic models of legged locomotion,” *Reg. Chaotic Dyn.*, vol. 13, pp. 267–282, 2008.
- [40] M. Raibert, K. Blankespoor, G. Nelson, and R. Playter, “BigDog team BigDog, the rough-terrain quadruped robot,” in *Proc. IFAC World Congr.*, 2008, pp. 10822–10825.
- [41] S. S. Roy and D. K. Pratihar, “Kinematics dynamics and power consumption analyses for turning motion of a six-legged robot,” *J. Intell. Robot. Syst.*, vol. 74, pp. 663–688, 2014.
- [42] J. Schmitt and P. Holmes, “Mechanical models for insect locomotion: Dynamics and stability in the horizontal Plane—II,” *Appl. Biol. Cybern.*, vol. 83, pp. 517–527, 2000.
- [43] S. Sefati *et al.*, “Mutually opposing forces during locomotion can eliminate the tradeoff between maneuverability and stability,” *Proc. Nat. Acad. Sci. USA*, vol. 110, pp. 18798–18803, 2013.
- [44] A. T. Spröwitz *et al.*, “Oncilla robot: A versatile open-source quadruped research robot with compliant pantograph legs,” *Front. Robot. AI*, vol. 19, 2018, Art. no. 67.
- [45] S. A. Stamper, S. Sefati, and N. J. Cowan, “Snake robot uncovers secrets to sidewinders’ maneuverability,” *Proc. Nat. Acad. Sci. USA*, vol. 112, pp. 5870–5871, 2015.
- [46] S. Steingrube, M. Timme, F. Wörgötter, and P. Manoonpong, “Self-organized adaptation of a simple neural circuit enables complex robot behaviour,” *Nature Phys.*, vol. 6, pp. 224–230, 2010.
- [47] S. H. Strogatz, *Nonlinear Dynamics and Chaos: With Applications to Physics, Biology, Chemistry, and Engineering*. New York, NY, USA: Perseus Books, 1994.
- [48] R. Takahashi and S. Inagaki, “Walk control of segmented multi-legged robot based on integrative control of legs and 2-DoF active intersegment joints,” *Adv. Robot.*, vol. 30, pp. 1354–1364, 2016.
- [49] G. K. Taylor and H. G. Krapp, “Sensory systems and flight stability: What do insects measure and why?,” *Adv. Insect Physiol.*, vol. 34, pp. 231–316, 2007.
- [50] K. Tsujita, H. Toui, and K. Tsuchiya, “Dynamic turning control of a quadruped locomotion robot using oscillators,” *Adv. Robot.*, vol. 19, pp. 1115–1133, 2005.
- [51] *Toshiba Corp.*, “Quadruped robot for nuclear facilities,” *E-J. Adv. Maintenance*, vol. 6, 2014, Art. no. NT64.
- [52] M. Vukobratović, B. Borovac, D. Surla, and D. Stokić, *Biped Locomotion: Dynamics, Stability, Control and Application*. New York, NY, USA: Springer-Verlag, 1990.
- [53] P. W. Webb, “Designs for stability and maneuverability in aquatic vertebrates: What can we learn?” in *Proc. Int. Symp. Unmanned Untethered Submersible Technol.*, 1997, pp. 86–108.
- [54] T. Wei, Q. Luo, Y. Mo, Y. Wang, and Z. Cheng, “Design of the three-bus control system utilising periodic relay for a centipede-like robot,” *Robotica*, vol. 34, pp. 1841–1854, 2016.
- [55] B. H. Wilcox *et al.*, “Athlete: A cargo handling and manipulation robot for the moon,” *J. Field Robot.*, vol. 24, pp. 421–434, 2007.
- [56] D. Zhao and S. Revzen, “Multi-legged steering and slipping with low DoF hexapod robots,” *Bioinspiration Biomimetics*, vol. 15, 2020, Art. no. 045001.
- [57] Y. Zhu, T. Guo, Q. Liu, Q. Zhu, X. Zhao, and B. Jin, “Turning and radius deviation correction for a hexapod walking robot based on an ant-inspired sensory strategy,” *Sensors*, vol. 17, 2017, Art. no. 2710.



**Shinya Aoi** (Member, IEEE) received the B.E., M.E., and Ph.D. degrees in engineering from the Department of Aeronautics and Astronautics, Kyoto University, Kyoto, Japan, in 2001, 2003, and 2006, respectively.

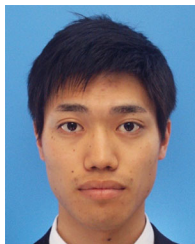
He was with Kyoto University from 2006 to 2022. He is currently a Professor with the Department of Mechanical Science and Bioengineering, Graduate School of Engineering Science, Osaka University, Osaka, Japan. His research interests include dynamics and control of legged robots and analysis and simulations of locomotion in humans and animals.

Dr. Aoi received the Young Scientists’ Prize, the Commendation for Science and Technology by the Minister of Education, Culture, Sports, Science and Technology, Japan, in 2017. He also received the Best Paper Award of IEEE RAS/EMBS International Conference on Biomedical Robotics and Biomechatronics in 2012, and the Best Paper Award of IEEE International Symposium on Micro-NanoMechatronics and Human Science in 2018. He was a Research Fellow (DC1) of the Japan Society for the Promotion of Science from 2003 to 2006.



**Ryo Tomatsu** received the B.E. and M.E. degrees in engineering from the Department of Aerospace Engineering, Osaka Prefecture University, Osaka, Japan, in 2017, and from the Department of Aeronautics and Astronautics, Kyoto University, Kyoto, Japan, in 2019, respectively.

He is currently with Fanuc Corporation, Yamanaishi, Japan. His research interests include the control of legged robots.



**Yuki Yabuuchi** received the B.E. and M.E. degrees in engineering from the Department of Mechanical Science and Bioengineering, Osaka University, Osaka, Japan, in 2018, and from the Department of Aeronautics and Astronautics, Kyoto University, Kyoto, Japan, in 2020, respectively.

He is currently with Shimano Inc., Osaka, Japan. His research interests include the control of legged robots.



**Daiki Morozumi** received the B.E. and M.E. degrees in engineering from the Department of Aeronautics and Astronautics, Kyoto University, Kyoto, Japan, in 2020 and 2022, respectively.

He is currently with Honda Motor Co. Ltd., Tokyo, Japan. His research interests include the control of legged robots.



**Kota Okamoto** received the B.E. and M.E. degrees in engineering, in 2019 and 2021, respectively, from the Department of Aeronautics and Astronautics, Kyoto University, Kyoto, Japan, where he is currently working toward the Ph.D. degree.

His research interests include dynamics and control of legged robots and analysis and simulations of locomotion in humans and animals.



**Soichiro Fujiki** (Member, IEEE) received the B.E., M.E., and Ph.D. degrees in engineering from the Department of Aeronautics and Astronautics, Kyoto University, Kyoto, Japan, in 2010, 2012, and 2015, respectively.

He was an Assistant Professor with the Department of Life Sciences, Graduate School of Arts and Sciences, The University of Tokyo, Tokyo, Japan, from 2015 to 2018. He is currently a Lecturer with the Department of Physiology, School of Medicine, Dokkyo Medical University, Tochigi, Japan, where he was an

Assistant Professor from 2018 to 2020. His research interests include dynamics and control of legged robots and analysis and simulations of locomotion in animals.

Dr. Fujiki was a Research Fellow (DC2, PD) of the Japan Society for the Promotion of Science from 2014 to 2015.



**Kei Senda** (Member, IEEE) received the M.S. degree in aeronautical engineering and the Ph.D. degree in engineering from Osaka Prefecture University, Osaka, Japan, in 1988 and 1993, respectively.

He was with Osaka Prefecture University and Kanazawa University, Kanazawa, Japan, from 1988 to 2008. Since 2008, he has been a Professor with the Department of Aeronautics and Astronautics, Graduate School of Engineering, Kyoto University, Kyoto, Japan. His current research interests include dynamics and control of aerospace systems, intelligence and autonomy for mechanical systems, and motion intelligence of animals.

Dr. Senda received the Best Presented Paper Award of the AIAA Guidance, Navigation, and Control Conference in 1992, the Best Paper Award of the Institute of Systems, Control and Information Engineers in 1994, the Best Paper of the Multiconference on Systemics, Cybernetics, and Informatics in 2003, and the Best Paper Award of IEEE RAS/EMBS International Conference on Biomedical Robotics and Biomechanics in 2012. He was also a finalist of the Best Conference Paper of IEEE International Conference on Systems, Man, and Cybernetics in 2011.



**Kazuo Tsuchiya** received the B.S., M.S., and Ph.D. degrees in engineering from Kyoto University, Kyoto, Japan, in 1966, 1968, and 1975, respectively.

From 1968 to 1990, he was a Research Member of the Central Research Laboratory, Mitsubishi Electric Corporation, Amagasaki, Japan. From 1990 to 1995, he was a Professor with the Department of Computer Controlled Machinery, Osaka University, Osaka, Japan. From 1995 to 2007, he was a Professor with the Department of Aeronautics and Astronautics, Kyoto University. In 2007, he retired from Kyoto

University and became a Professor Emeritus of Kyoto University. From 2008 to 2013, he was a Professor with the Department of Mechanical Engineering, Doshisha University, Kyoto. His research interests include dynamic analysis, guidance, and control of space vehicles, and nonlinear system theory for distributed autonomous systems.

Dr. Tsuchiya received the Asahi Prize for Spacecraft "Hayabusa" Project Team as a representative of academia in 2011 and the Best Paper Award of IEEE RAS/EMBS International Conference on Biomedical Robotics and Biomechanics in 2012.